

E19-2013-17

Kh. T. Kholmurodov<sup>1,2</sup>, E. B. Dushanov<sup>1,3</sup>,  
E. A. Krasavin<sup>1,2</sup>, H. K. Hassan<sup>4</sup>, H. A. ElHabashy<sup>5</sup>,  
A. Galal<sup>4</sup>, N. H. Sweilam<sup>6</sup>, K. Yasuoka<sup>7</sup>

MOLECULAR DYNAMICS SIMULATIONS  
OF THE **DNA** INTERACTION WITH METALLIC  
NANOPARTICLES AND TiO<sub>2</sub> SURFACES

Submitted to the Proceedings of the 5th Japan–Russia International  
Workshop MSSMBS'12, September 9–12, 2013, Dubna, Russia

---

<sup>1</sup> Laboratory of Radiation Biology, JINR, Dubna, Russia

<sup>2</sup> Dubna International University, Dubna, Russia

<sup>3</sup> Institute of Nuclear Physics, Ulugbek, Tashkent, Uzbekistan

<sup>4</sup> Chemistry Department, Faculty of Science, Cairo University, Cairo, Egypt

<sup>5</sup> Physics Department, American University in Cairo, Cairo, Egypt

<sup>6</sup> Mathematics Department, Faculty of Science, Cairo University, Cairo,  
Egypt

<sup>7</sup> Department of Mechanical Engineering, Keio University, Minato, Tokyo,  
Japan

Молекулярно-динамические моделирования взаимодействия ДНК с металлическими наночастицами и поверхностями TiO<sub>2</sub>

Понимание механизмов взаимодействия и связывания молекулы ДНК с металлическими наночастицами (НЧ) и поверхностями представляет огромный интерес в современных медицинских приложениях в связи с диагностикой и терапией онкологических заболеваний. Недавние экспериментальные и теоретические исследования включают в себя взаимодействия высоколокализованных протонных лучей или металлических НЧ (таких как Ag, Au и т. п.), нацеленных на терапию онкологических заболеваний посредством инъекции металлических микро- или наночастиц в опухолевых тканях с последующим локальным микроволновым или лазерным нагревом. Эффекты мутационных структурных изменений в ДНК или белках могут выражаться в разрушении природных химических (водородных) связей или, наоборот, в создании новых связей, не существующих в исходной структуре. Причиной подобных изменений может быть замена одного нуклеотида на другой (в ДНК) или замещение специфических аминокислотных остатков (в белках), которые и приводят к большим структурным перестройкам или неправильным укладкам. На атомно-молекулярном уровне замещение одного нуклеотида на другой (в двухнитевых цепочках ДНК) или замена одной аминокислоты на другую (в белках) вызывает существенную модификацию их молекулярного поля, что приводит к разрушению локально важных водородных связей, отвечающих за структурную стабильность биологических молекул. В молекулярно-динамических исследованиях представлены четыре модели ДНК, а также выявлена гибкость пуриновых и пиримидиновых нуклеотидов в процессе их взаимодействия с металлическими НЧ и поверхностями TiO<sub>2</sub>.

Работа выполнена в Лаборатории радиационной биологии ОИЯИ.

Препринт Объединенного института ядерных исследований. Дубна, 2013

Molecular Dynamics Simulations of the DNA Interaction with Metallic Nanoparticles and TiO<sub>2</sub> Surfaces

The understanding of the mechanism of DNA interactions and binding with metallic nanoparticles (NPs) and surfaces represents a great interest in today's medicine applications due to diagnostic and treatment of oncology diseases. Recent experimental and simulation studies involve the DNA interaction with highly localized proton beams or metallic NPs (such as Ag, Au, etc.), aimed at targeted cancer therapy through the injection of metal micro- or nanoparticles into the tumor tissue with consequent local microwave or laser heating. The effects of mutational structure changes in DNA and protein structures could result in destroying of native chemical (hydrogen) bonds or, on the contrary, creating of new bonds that do not normally exist there. The cause of such changes might be the alteration of one or several nucleotides (in DNA) or the substitution of specific amino acid residues (in proteins) that can lead to the essential structural destabilization or unfolding. At the atomic or molecular level, the replacement of one nucleotide by another (in DNA double helices) or replacement of one amino acid residue by another (in proteins) cause essential modifications of the molecular force fields of the environment that break locally important hydrogen bonds underlying the structural stability of the biological molecules. In this work, the molecular dynamics (MD) simulations were performed for four DNA models and the flexibilities of the purine and pyrimidine nucleotides during the interaction process with the metallic NPs and TiO<sub>2</sub> surface were clarified.

The investigation has been performed at the Laboratory of Radiation Biology, JINR.

Preprint of the Joint Institute for Nuclear Research. Dubna, 2013

## INTRODUCTION

The effects of mutational structure changes in biological objects (such as DNA, proteins, and so on) have mostly associated with different kinds of diseases that take place at physiological conditions. In human body, for example, the origins of many diseases correlate with the malfunctioning of DNA or proteins, followed by their structural perturbation, improper conformational behavior or unfolding. The induced mutations in biological molecules (DNA, proteins, etc.) have quite a different nature (environmental factors and viruses, ionizing radiation and mutagenic chemicals, inherited genetic alterations, and so on). Point mutations in DNA and protein structures could result in destroying of native chemical (hydrogen) bonds or, on the contrary, creating of new bonds that do not normally exist there. The cause of such changes might be the alteration of one or several nucleotides (in DNA) or the substitution of specific amino acid residues (in proteins), that can lead to the essential structural destabilization or unfolding. At the atomic or molecular level, the replacement of one nucleotide by another (in DNA double helices) or replacement of one amino acid residue by another (in proteins) cause essential modifications of the molecular force fields of the environment that break locally important hydrogen bonds underlying the structural stability of the biological molecules. As a result, we get global structure changes of the biomolecule, which make their functional behaviour different from that of the native ones. In other words, a specific disease (say, cancer) can develop if the biomolecules (DNA, protein) become unable to perform their function [1–3].

High-power beams of particle accelerators (like JINR nuclear facilities in Dubna, Russia) provide a wide basis for the investigation of the mutagenic effect of ionizing radiation. The radiation genetics and radiobiology research objects include the mechanism of the induction of mutations of different nature by ionizing radiation. In some aspects, computer molecular simulation and analysis appear to be an extremely efficient tool for supporting various biophysical, biochemical or radiobiological experiments. The modern molecular dynamics approach should be specially mentioned, which is widely applied in today's biophysics, radiobiological and materials science research. In the present work, based on the advanced molecular dynamics methods and visualization techniques, we simulate the behaviour of native and mutated DNA interacting with metallic nanoparticles and surface [1–13].

Using molecular dynamics (MD) simulation technique we were aimed to elucidate the important DNA–metal interaction mechanism in two closely correlated aspects:

- 1) The DNA–metallic nanoparticles (NPs) binding;
- 2) The DNA–metallic oxide surface interaction.

Firstly, the MD study was performed to investigate the physical and molecular mechanism of the interaction of nano- and microparticles with DNA (a native double-helix chain and its several mutated versions — on the one end, on minor and major grooves). It is worth noting that understanding the mechanism of DNA–NP (nanoparticle) interaction represents a great interest in today's medicine applications due to diagnostics and treatment of oncology diseases. Some recent experimental and simulation studies involve the interaction of DNA with highly localized high power beams and various nanoparticles (Ag, Au, etc.), which were aimed at targeted cancer therapy through the injection of metal micro- or nanoparticles into the tumor tissue with consequent local microwave or laser heating. One has to mention some activities on using of nuclear medicine facilities operating at JINR that are performed for the above purposes by the JINR's Laboratory of Radiation Biology (under the guidance of Academy corr.-mem. Krasavin E. A.).

Secondly, one extend the DNA–nanoparticles interaction to DNA–surface by simulating the interaction of DNA with metal oxide ( $\text{TiO}_2$ ). It is well known that titanium dioxide ( $\text{TiO}_2$ ) has a valuable variety of applications in a lot of different areas such as heterogeneous catalysis and photocatalysis, sensoristics, cosmetics, sunscreen, toothpaste, coating, etc. Ti as a metal has a good biocompatibility due to unique characteristics such as lightness, excellent mechanical properties, lack of toxicity, and extremely low corrosion rate. These properties make it suitable for use as a medical implant and prosthesis material [14]. Titanium surface reacts spontaneously with air and biological solutions forming an inert thin oxide layer (0.5–10 nm thick) that is crucial for molecular recognition [15]. Titanium dioxide ( $\text{TiO}_2$ ) is a naturally occurring metal oxide mineral while  $\text{TiO}_2$  nanoparticles are manufactured artificially in large quantities. However, the synthesis and applications of titanium dioxide nanoparticles ( $\text{TiO}_2$  NPs) are increasing due to their distinctive physico-chemical characteristics, and increased industrial and medical applications. The consistently expanding usage of  $\text{TiO}_2$  and  $\text{TiO}_2$  NPs has evoked urgent concern about their potential health effect. Although,  $\text{TiO}_2$  is chemically inert,  $\text{TiO}_2$  NPs can cause negative health effects so that the biological responses to NPs may exceed those of micron-sized particles. Because of their small size which do not exceed a hundred nanometers at maximum, high number per given mass, large specific surface area, and generation of free radicals, NPs can penetrate cells and influence several subcellular mechanisms. Some studies report that nanoparticles may defuse and penetrate into cell nuclei and may directly or indirectly affect the structure and function of DNA [16–19].

TiO<sub>2</sub> NPs may directly or indirectly damage DNA through interactive oxidative stress and/or inflammatory responses. One *in vivo* study illustrates that TiO<sub>2</sub> NPs induce genotoxicity, oxidative DNA damage, and inflammation in a mice model while other *in vitro* shows that it can produce a significant induce cyto- and genotoxicity in cultured Wistar Institute, Susan Hayflick (WISH) cells. On the one hand, some studies proved that there is a kind of direct chemical interaction between TiO<sub>2</sub> NPs and DNA, through the DNA phosphate group, but no direct evidence for the mutagenesis. On the other hand, TiO<sub>2</sub> NPs can cause indirect DNA damage through inflammation and generation of reactive oxygen species (ROS) that is principally the main reason for tumor induction. Additionally, in [20], it was revealed that TiO<sub>2</sub> NPs decrease the reduced nicotinamide adenine dinucleotide (NADH) levels and impair membrane potential and mitochondrial function accompanied by ROS generation during mitochondrial respiration. TiO<sub>2</sub> has recently been reclassified by the international agency for research on cancer (IARC) as group 2B carcinogen. In [21], it is mentioned that genotoxicity studies that measure different types of DNA damage (e.g., gene mutations, chromosomal damage, and DNA strand break formation) are an important part of cancer research and risk assessment of potential carcinogens. Thus, mutation in the recognition part of a DNA generally causes alterations in its protein binding affinity that alter on their physiological functions. The mutation may cause considerable structural change particularly the groove width in the DNA as well as the interactions at the DNA-protein interface may be weakened considerably due to mutation [16–19, 22–25].

## 1. MATERIALS AND METHODS

A classical molecular dynamics study was performed using the DL\_POLY\_4.03.3 [26] general-purpose code. The NVT ensemble at  $T = 298$  K with a Nosé–Hoover thermostat and Verlet leapfrog scheme were employed. To calculate the long-range electrostatic forces, three-dimensional Ewald summation with the automatic optimization parameter  $f = 1.0 \cdot 10^{-4}$  and convergence parameter  $0.24375 \text{ \AA}^{-1}$  was used. The integration time step of the dynamic equations of motion was 1 fs.

All the initial and mutated DNA configurations were created using the Amber Tools LEaP basic preparation program [4, 5]. The DNA was solvated with water (TIP3P) molecules [27] produced in spherical and rectangular (periodic) water baths. In creating the force field parameters the combination of CHARMM and «general Amber force field (GAFF)» databases [4, 5, 28] were employed.

The DNA–water system were equilibrated at normal (room) temperature and located between two TiO<sub>2</sub> (anatase) surfaces. The MD cell volume of the DNA–water–TiO<sub>2</sub> system was as  $V = (37.85, 56.775, 57.639) \text{ \AA}^3$ . (The only DNA–

**Table 1. The force field potentials and parameters for TiO<sub>2</sub> surface**

| Buckingham potential: $A_{ij} \exp(-r_{ij}/\rho_{ij}) - C_{ij}/r_{ij}^6$ |                   |            |                                     |
|--|-------------------|------------|-------------------------------------|
| $l - j$  | $A_{ij}$ (kJ/mol) | $\rho$ (Å) | $C_{ij}$ (kJ/mol · Å <sup>6</sup> ) |
| Ti-Ti  | 3004646.13432     | 0.154      | 506.54433                           |
| Ti-O   | 1637244.37188     | 0.194      | 1214.7449                           |
| O-O  | 1137621.80484     | 0.234      | 2915.7794                           |

water volume was 70463.018 Å<sup>3</sup>; its total mass 28431.872 a.m.u.; so the density was equal to 0.670 g/cc).

The water atoms were constrained using the SHAKE method [29].

For the TiO<sub>2</sub> surfaces, the force fields as reported by Kavathekar et al. [30] and Guillot et al. [31] were used. The potential parameters for TiO<sub>2</sub> surface were developed by Matsui and Akaogi [32]. Unit cell parameters for TiO<sub>2</sub> model were taken from the EIM databases supported by the Russian Foundation for Basic Research [33]. Table 1 represents the Buckingham (buck) potential parameters used for the TiO<sub>2</sub> surface [32].

The results of simulations and images of the molecular systems were analyzed by the Visual Molecular Dynamics (VMD) [7] software.

## 2. RESULTS AND DISCUSSION

The MD simulation results below cover the following model systems: 1) The DNA-metallic nanoparticles (NPs) binding; 2) The DNA-metallic oxide surface interaction. The details of the MD simulations are given in Sec. 1.

**2.1. The DNA-Metallic NP Interactions.** First, we have generated a spherical water bath embedding the DNA and a small metallic NP. The DNA and water (TIP3P) model parameters were taken from the standard AMBER database. As for the NP, the force field parameters for the gold atoms were used. We have generated several DNA-water-NP configurations with single, two, three-five atomic sites to mimic various small nanoparticle clusters. In Fig. 1, a snapshot of the DNA chain and metallic nanoparticle (NP) surrounded by water is presented.

We have generated multiple DNA-water-NP configurations and equilibrated all models at a normal (room) temperature  $T = 300$  K. The initial positions of the DNA and NP inside the water bath were well-separated and well-distinguished. The total molecular systems under considerations next to undergo a long-nano-second relaxation procedure up to 10-12 ns. In Fig. 2, six sequential snapshots on the DNA molecule interacting with NP are presented.

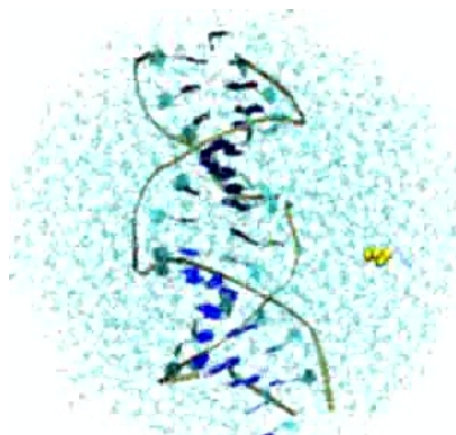


Fig. 1. A DNA chain embedded by water and interacting with metallic nanoparticle (NP). The DNA is shown as ribbon structure, water — as a blue bath; NP — as golden balls

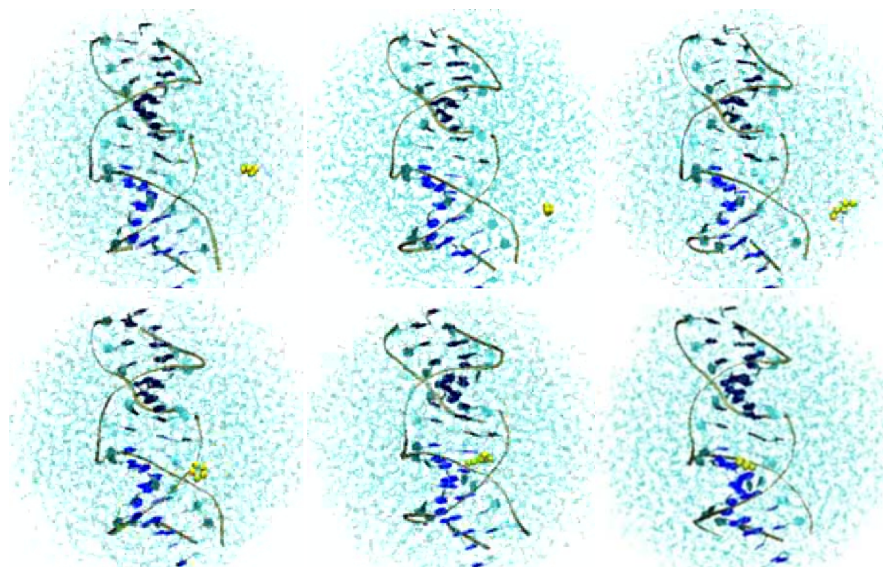


Fig. 2. Six sequential snapshots on DNA–water–NP interaction process (from left to right). The DNA conformation behaves stable till the NP is captured by a DNA minor groove

During the long-nanosecond dynamics, the metallic NPs would continuously change their positions, approaching the DNA molecule from its different sides (from the DNA ends, the DNA minor and major grooves, etc.), thereby seeking a

preferable binding site. One of the events of the DNA–NP binding is graphically illustrated in Fig. 3.

Until NP binds to DNA, the DNA conformation behaves stable and it does not change visibly in comparison with the starting one. In Fig. 3, we can see that within  $t \approx 1.5 - 2$  ns, from the start of the equilibration dynamics the NP is localized at a DNA minor groove. From this stage of a DNA–NP close contact (bond) formation, the DNA structure undergoes a substantial deformation. The shape of the DNA molecule would continuously change in correlation with the NP capture and formation of a close contact. In Fig. 3, the changes on a relative DNA unit size are shown separately (right  $Y$  axis); it is seen that the dynamical changes on the DNA size following by the capture of NP vary from 17 to 26%.

The process of the DNA dynamical size change is presented separately in Fig. 4, where the DNA conformational modifications after the capture of NP by DNA minor groove are shown.

Based on the above observations, one can conclude that different parts of the DNA molecule have likely to possess a different flexibility with regard to an efficient capturing of metallic NPs and interaction with. Say, from the above results one observes that an efficient NP–DNA interaction has preferably localized on a DNA minor groove segment. So, next we performed the MD simulations and some energetics estimations on the only DNA chain solvated

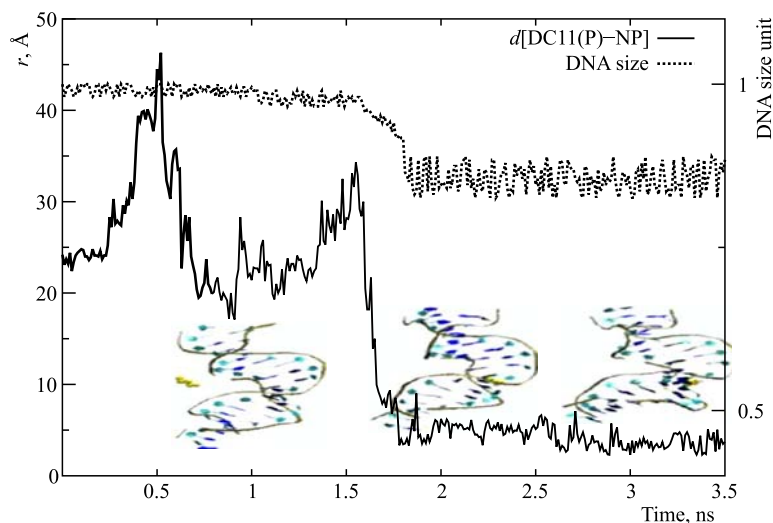


Fig. 3. A distance diagram displaying the NP trajectories and formation of DNA–NP close bonding contact. The DNA is shown as ribbon structure, NP — as golden balls. Right  $Y$  axis demonstrates the DNA longitudinal size deformation correlated with the capture of NP by a DNA minor groove

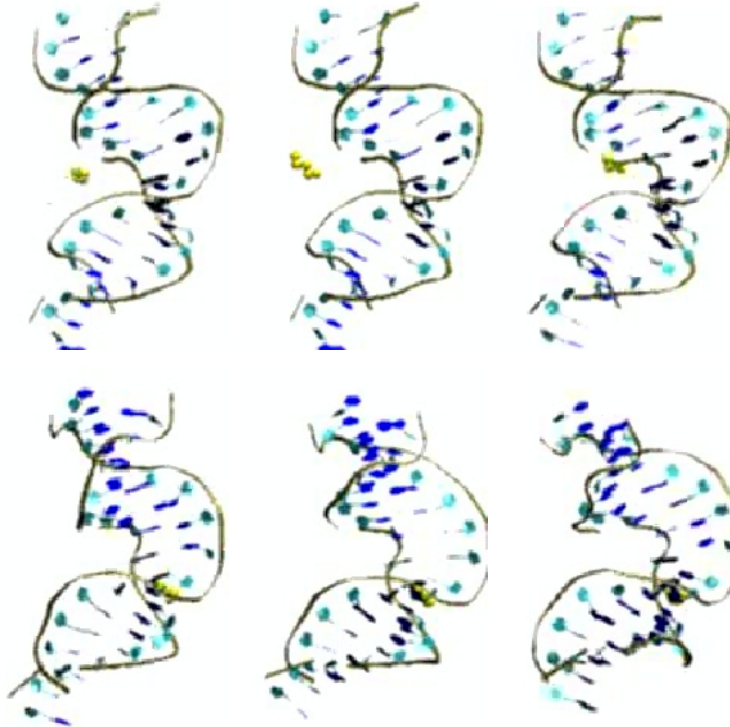


Fig. 4. Six sequential snapshots of the DNA interacting with NP (from left to right). The process of the DNA conformation changes with NP capture is shown

in water, but without any nanoparticle (NP) inclusion into consideration. Figure 5 and Table 2 show four DNA models simulated with water as in Figs. 1 and 2. We have introduced these DNA models as: model m0 — native structure; model m1 — G1C and C20G mutations (G/C → C/G); model m2 — A6C and T15G mutations (A/T → C/G); model m3 — T4G and A17C mutations (T/A → G/C)

**Table 2. The DNA models described as in Fig. 5 are numbered and sequenced as follows: model m0: no mutation; model m1: G1C and C20G mutations (G/C → C/G); model m2: A6C and T15G mutations (A/T → C/G); model m3: T4G and A17C (T/A → G/C) mutations**

|                        |                  |                  |                  |    |    |    |    |    |    |    |    |   |
|------------------------|------------------|------------------|------------------|----|----|----|----|----|----|----|----|---|
| DNA chain numbering: { |                  | 1                | 2                | 3  | 4  | 5  | 6  | 7  | 8  | 9  | 10 | } |
|                        |                  | 11               | 12               | 13 | 14 | 15 | 16 | 17 | 18 | 19 | 20 | } |
| Model m0:              | Model m1:        | Model m2:        | Model m3:        |    |    |    |    |    |    |    |    |   |
| 5'-GCGTTAACGC-3'       | 5'-CCGTTAACGC-3' | 5'-GCGTTCACGC-3' | 5'-GCGGTAACGC-3' |    |    |    |    |    |    |    |    |   |
| 3'-CGCAATTGCG-5'       | 3'-GGCAATTGCG-5' | 3'-CGCAAGTGCG-5' | 3'-CGCCATTGCG-5' |    |    |    |    |    |    |    |    |   |

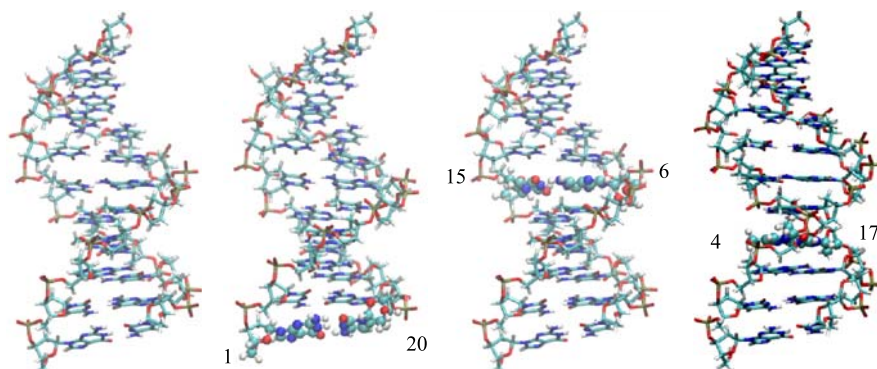


Fig. 5. Four models of DNA simulated with water as in Figs.1 and 2. From the left to right: model m0 — native structure; model m1 — G1C and C20G (G/C → C/G) mutations; model m2 — A6C and T15G (A/T → C/G) mutations; model m3 — T4G and A17C (T/A → G/C) mutations

ibility of different segments of the DNA molecule (the DNA ends, minor and major grooves). For better understanding of the influence of the induced mutations with respect to the DNA native one, we have run molecular dynamics simulations on the four DNA models, each solvated with the same number of water molecules. In Fig.6, the total energy vs. time is drawn for each of the DNA–water models. The two curves in Fig.6 demonstrate that models m0 (native DNA) and m1 (DNA chain mutated on the one end) have a comparable energetics behavior. At the same time, the third and the fourth DNA–water models, m2 and m3, show a relative significant decrease in energy than the native m0 and m1 ones. One has to stress out that mutations in the models m2 and m3 are located at the DNA major and minor grooves, respectively.

Let us estimate the thermodynamic stabilities of these four DNA models with respect to the induced mutations as shown in Table 2. It is well known that thermodynamic stability of DNA double helix depends on its length where longer molecules are more stable, its GC-content and sequence since stacking are sequence specific. The four DNA models under investigation are ten bases pairs in length, so their energetic stabilities due to length dependency are expected to be similar and cannot be used as a point of comparison [19]. On the other hand, hydrogen bonds between base pairing nucleotides are the main reason where higher GC-content (%) is energetically favorable for DNA molecules. This is why different base pairing nucleotides form different numbers of hydrogen bonds. AT base pair forms two hydrogen bonds, while GC forms three hydrogen

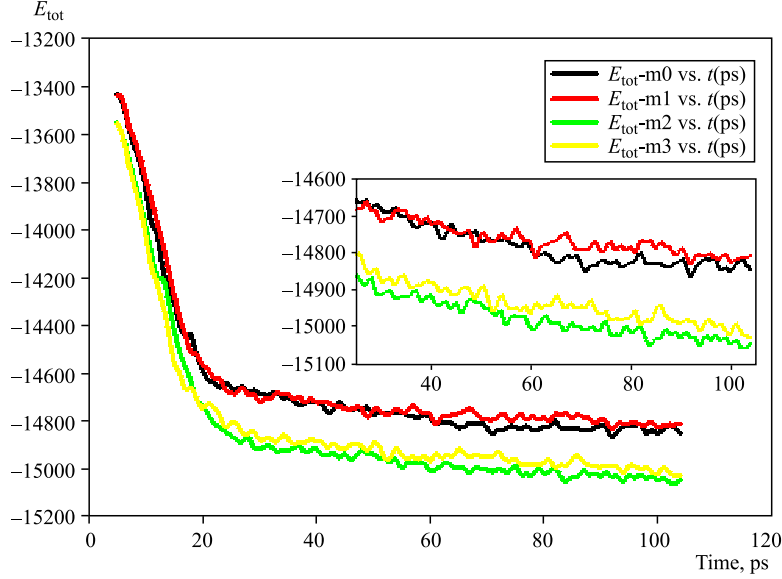


Fig. 6. This graph shows the total evaluated energies from the MD simulation results for four different models of solvated DNA

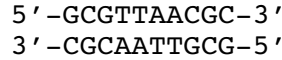
bonds. DNA with high GC-content is more thermodynamic stable and would have lower energy than DNA with lower GC-content. Calculating the GC-content percentages of our models, we have found that the first native DNA, m0, and the chain end mutated DNA, m1, have the same GC-content which is 60%, while the third major groove mutated DNA, m2, and the fourth minor groove mutated DNA, m3, have the same GC-content which is 70%. Both the GC base pairs content and the overall length of a DNA can determine the strength of the association between the two strands of DNA. Since the four DNA models have the same length, models with higher GC-content have stronger-interacting strands among other models. Moreover, calculating predicted values of the total energies of our models individually considering the nucleobases pairing and stacking (attractive, non-covalent interactions between aromatic rings) upon one another to form the helical structure of DNA will be done using the nearest neighbor (NN) parameters for Watson–Crick base pairs in 1 M NaCl. The published Watson–Crick NN parameters have been critically reviewed many times in literature and have great reliability. The total Gibbs free energy for the models can be calculated using the following equation:

$$\Delta G_{37(\text{tot})}^0 = \Delta G_{37(\text{int})}^0 + \Delta G_{37(\text{sym})}^0 + \sum \Delta G_{37(\text{st})}^0, \quad (1)$$

where  $\sum \Delta G_{37(st)}^0$  is the summation of the standard free-energy changes for the 10 possible Watson–Crick NNs and  $\Delta G_{37(int)}^0$  accounts for differences between duplexes with terminal AT vs. terminal GC pairs,  $\Delta G_{37(sym)}^0$  equals 10.43 kcal/mol if the duplex is self-complementary and equals zero if it is non-self-complementary. All estimated values of the energy have been measured at 37 °C which is the physiological temperature of human. It is clear that the values  $\Delta G_{37(int)}^0$  and  $\Delta G_{37(sym)}^0$  for our non-complementary structures will be the same for the four models, and  $\sum \Delta G_{37(st)}^0$  will be the main reason of the energy fluctuation between the four models [16, 18].

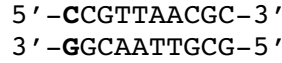
The calculated values of the  $\sum \Delta G_{37(st)}^0$  for the four DNA models are summarized below.

The first native model m0 (no mutation):



$$\begin{aligned} \Delta G_{37(tot,m0)}^0 &= \Delta G_{37(int)}^0 + \Delta G_{37}^0 \begin{pmatrix} G & C \\ C & G \end{pmatrix} + \Delta G_{37}^0 \begin{pmatrix} C & G \\ G & C \end{pmatrix} + \\ &+ \Delta G_{37}^0 \begin{pmatrix} G & T \\ C & A \end{pmatrix} + \Delta G_{37}^0 \begin{pmatrix} T & T \\ A & A \end{pmatrix} + \Delta G_{37}^0 \begin{pmatrix} T & A \\ A & T \end{pmatrix} + \Delta G_{37}^0 \begin{pmatrix} A & A \\ T & T \end{pmatrix} + \\ &+ \Delta G_{37}^0 \begin{pmatrix} A & C \\ T & G \end{pmatrix} + \Delta G_{37}^0 \begin{pmatrix} C & G \\ G & C \end{pmatrix} + \Delta G_{37}^0 \begin{pmatrix} G & C \\ C & G \end{pmatrix} + \\ &+ \Delta G_{37(sym)}^0 = 1.96 - 2.24 - 2.17 - 1.44 - 1.00 - 0.58 - \\ &- 1.00 - 1.44 - 2.17 - 2.24 + 0.00 = -12.32 \text{ kcal/mol.} \end{aligned}$$

The chain end mutated model m1 (mutated G1C and C2G):



$$\begin{aligned} \Delta G_{37(tot,m1)}^0 &= \Delta G_{37(int)}^0 + \Delta G_{37}^0 \begin{pmatrix} C & C \\ G & G \end{pmatrix} + \Delta G_{37}^0 \begin{pmatrix} C & G \\ G & C \end{pmatrix} + \\ &+ \Delta G_{37}^0 \begin{pmatrix} G & T \\ C & A \end{pmatrix} + \Delta G_{37}^0 \begin{pmatrix} T & T \\ A & A \end{pmatrix} + \Delta G_{37}^0 \begin{pmatrix} T & A \\ A & T \end{pmatrix} + \Delta G_{37}^0 \begin{pmatrix} A & A \\ T & T \end{pmatrix} + \\ &+ \Delta G_{37}^0 \begin{pmatrix} A & C \\ T & G \end{pmatrix} + \Delta G_{37}^0 \begin{pmatrix} C & G \\ G & C \end{pmatrix} + \Delta G_{37}^0 \begin{pmatrix} G & C \\ C & G \end{pmatrix} + \\ &+ \Delta G_{37(sym)}^0 = 1.96 - 1.84 - 2.17 - 1.44 - 1.00 - 0.58 - \\ &- 1.00 - 1.44 - 2.17 - 2.24 + 0.00 = -11.92 \text{ kcal/mol.} \end{aligned}$$

The major groove mutated model m2 (mutated A6C and T15G):



$$\begin{aligned} \Delta G_{37(\text{tot}, \text{m2})}^0 &= \Delta G_{37(\text{int})}^0 + \Delta G_{37}^0 \begin{pmatrix} G & C \\ C & G \end{pmatrix} + \Delta G_{37}^0 \begin{pmatrix} C & G \\ G & C \end{pmatrix} + \\ &+ \Delta G_{37}^0 \begin{pmatrix} G & T \\ C & A \end{pmatrix} + \Delta G_{37}^0 \begin{pmatrix} T & T \\ A & A \end{pmatrix} + \Delta G_{37}^0 \begin{pmatrix} T & C \\ A & G \end{pmatrix} + \Delta G_{37}^0 \begin{pmatrix} C & A \\ G & T \end{pmatrix} + \\ &+ \Delta G_{37}^0 \begin{pmatrix} A & C \\ T & G \end{pmatrix} + \Delta G_{37}^0 \begin{pmatrix} C & G \\ G & C \end{pmatrix} + \Delta G_{37}^0 \begin{pmatrix} G & C \\ C & G \end{pmatrix} + \\ &+ \Delta G_{37(\text{sym})}^0 = 1.96 - 2.24 - 2.17 - 1.44 - 1.00 - 1.28 - 1.45 - \\ &- 1.44 - 2.17 - 2.24 + 0.00 = -13.47 \text{ kcal/mol.} \end{aligned}$$

The minor groove mutated model m3 (mutated T4G and A17C):



$$\begin{aligned} \Delta G_{37(\text{tot}, \text{m3})}^0 &= \Delta G_{37(\text{int})}^0 + \Delta G_{37}^0 \begin{pmatrix} G & C \\ C & G \end{pmatrix} + \Delta G_{37}^0 \begin{pmatrix} C & G \\ G & C \end{pmatrix} + \\ &+ \Delta G_{37}^0 \begin{pmatrix} G & G \\ C & C \end{pmatrix} + \Delta G_{37}^0 \begin{pmatrix} G & T \\ C & A \end{pmatrix} + \Delta G_{37}^0 \begin{pmatrix} T & A \\ A & T \end{pmatrix} + \\ &+ \Delta G_{37}^0 \begin{pmatrix} A & A \\ T & T \end{pmatrix} + \Delta G_{37}^0 \begin{pmatrix} A & C \\ T & G \end{pmatrix} + \Delta G_{37}^0 \begin{pmatrix} C & G \\ G & C \end{pmatrix} + \Delta G_{37}^0 \begin{pmatrix} G & C \\ C & G \end{pmatrix} + \\ &+ \Delta G_{37(\text{sym})}^0 = 1.96 - 2.24 - 2.17 - 1.84 - 1.44 - 0.58 - 1.00 - \\ &- 1.44 - 2.17 - 2.24 + 0.00 = -13.16 \text{ kcal/mol.} \end{aligned}$$

The predicted energy values with the nearest neighbor (NN) parameters for Watson–Crick base pairs in 1 M NaCl gave us a general view about the energetic and stability statuses of the models. Fortunately, the above MD simulation results for the four DNA molecules give us matching outputs with the predicted orders for the four model’s energies. One has to note that there is an approximate constant shift in energy values evaluated from MD simulations than that evaluated from the calculations. One can relate it to the water path energy contribution in the total energy of the DNA–water system. To prove this assumption, we have run molecular dynamics for the water molecules alone with the same particles number and simulation parameters as used for solvated DNA models. It matches

positively with our assumption that the water energy has approximate constant shift effect on the total energy of the four solvated DNA models. Thus, the predicted energy values and the evaluated energy from the MD simulation results indicate that model **m2** has the lowest energy,  $\Delta G_{37(\text{tot},\text{m}2)}^0$ , and the highest thermodynamic stability among other models followed by model **m3**,  $\Delta G_{37(\text{tot},\text{m}3)}^0$ , then by model **m0**,  $\Delta G_{37(\text{tot},\text{m}0)}^0$ , finally by model **m1**,  $\Delta G_{37(\text{tot},\text{m}1)}^0$ , which has the highest energy and the lowest stability among the other models. The native DNA (model **m0**) and the DNA chain end mutated (model **m1**) structures have close predicted energy values. The DNA **m2** and **m3** models have relatively lower energy values than that of **m0** and **m1** ones. So far, the DNA major and minor groove mutated models seem to possess the most favorable energetic characteristics for the specific stacked sequence under consideration. Such an energetic behavior makes a sense due to DNA–metallic NPs binding phenomena as reported above. The DNA mutated sites may cause an essential modification of the DNA–NPs interaction; obviously, this might be important to be taken into account for a number of similar reactions in the applied or experimental realizations.

**2.2. The DNA–Metallic Oxide Surface Interactions.** In this section, we extend the DNA–metallic NPs interaction to DNA–surface one by simulating the interaction of DNA with metal oxide (titanium oxide,  $\text{TiO}_2$ ).

Four DNA structures as described in the previous section were solvated by water and located in between two symmetrically  $\text{TiO}_2$  surfaces as shown in Fig. 7. The DNA–water– $\text{TiO}_2$  models were equilibrated at a room temperature

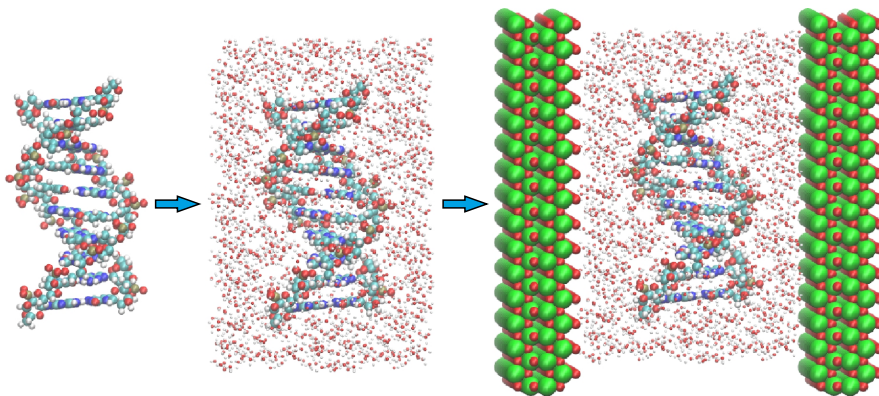


Fig. 7. (Color on-line). The initial DNA configuration (left) embedded in water (middle) and surrounded (right) by two symmetrically  $\text{TiO}_2$  surfaces (walls) are shown. The titanium (Ti) atoms are shown as large green balls; oxygen (O) atoms — as small red balls

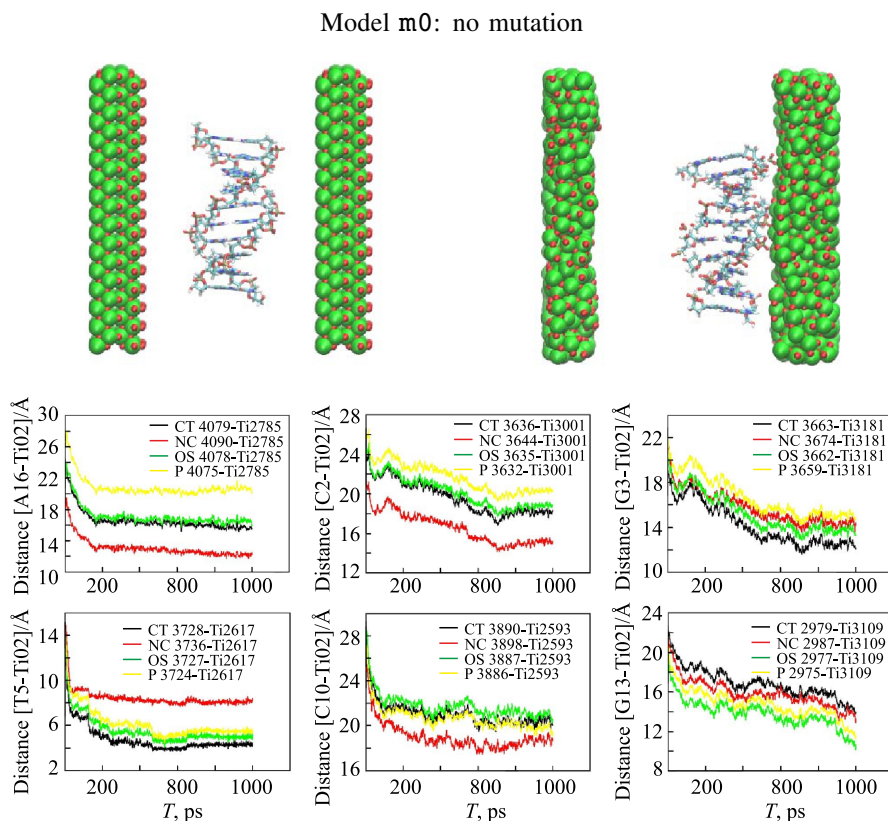


Fig. 8. The initial and final DNA configurations for model m0 (no mutation) as well as for the RMSD graphs are shown

under similar environmental and thermodynamical parameters (see Sec. 1) and after reaching the equilibrated states we have picked up for each of four models the DNA–surface distance distribution statistics (Figs. 8–11).

In Figs. 8–11, the DNA–TiO<sub>2</sub> distance graphs were calculated by fixing a certain Ti atom on TiO<sub>2</sub> surface and measuring the distance between it and the closest backbone atoms of DNA (C, N, O and P) for each of the four nucleotides A, C, G and T. We also calculated the DNA–surface distance distributions by taking into account the position of the nucleotides on the DNA double strand. So that, we used three different positions for each nucleotide to predict a general picture with a lower error that may result from the uncertainties (say, due to possible fluctuations in the position changing or in nucleotide sites relative to the whole DNA double strand).

Model m1: G1C and C20G mutations

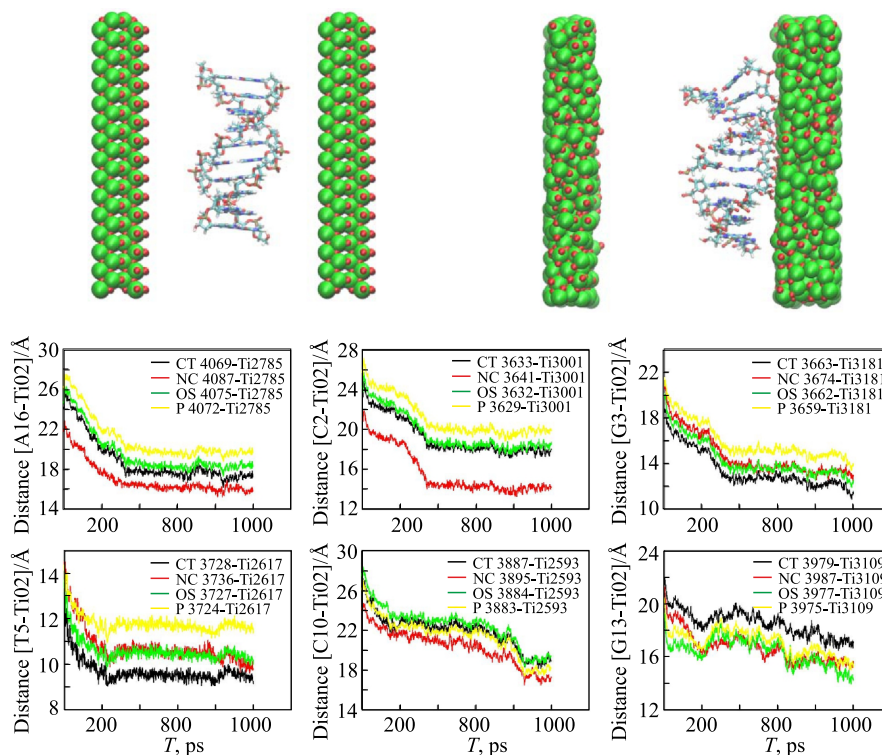


Fig. 9. The initial and final DNA configurations for model m1 (G1C and C20G mutations) as well as for the RMSD graphs are shown

In Figs. 8–11, the DNA–TiO<sub>2</sub> distance distributions together with the snapshots of initial and final states are presented for all simulated structures (m0, m1, m2, and m3), respectively. From Fig. 8, representing the DNA–TiO<sub>2</sub> distances for the native structure (model m0), we can say that in average the closest atom to the surface is nitrogen atom which is matching with the chemistry of coordination bonding. As is known, Ti ion in TiO<sub>2</sub> still has vacant orbitals which facilitate the interaction with donor atoms such as nitrogen, oxygen and phosphorous due to their lone pair of electrons. This Lewis acid–Lewis base interaction between donor atoms of DNA and Ti ion promotes some conformational changes of the DNA as predicted from the distance graphs shown in Fig. 8. The large decreasing in the distance distribution with time indicates that the structure has lost its original conformation due to the interaction with TiO<sub>2</sub>. On the other

### Model m2: A6C and T15G mutations

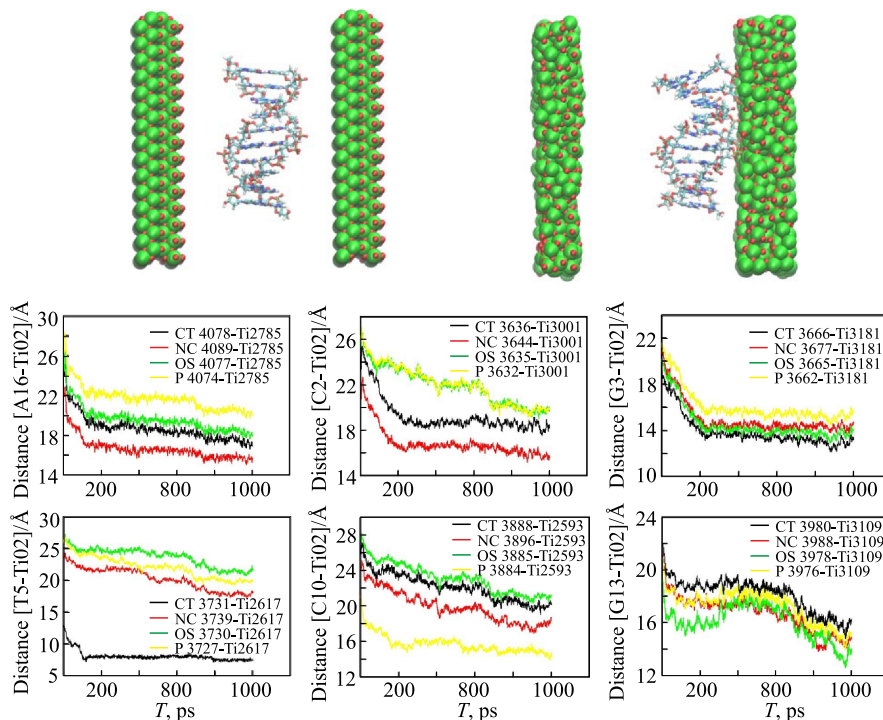


Fig. 10. The initial and final DNA configurations for model m2 (A6C and T15G mutations) as well as for the RMSD graphs are shown

hand, a high degree of fluctuations in the distance distribution graphs is another indicator for the conformational change of m0 structure.

It is likely that the induced mutations on DNA structure have to affect the DNA binding ability with a  $\text{TiO}_2$  surface. So that, the changes in the DNA-surface distances could be a good indicator to distinguish the effect of mutation. The DNA- $\text{TiO}_2$  distance distribution graphs for m1, m2 and m3 models are shown in Figs. 9–11, respectively. By comparing the distance distribution graphs between the three mutated structures and that of the native one, we can observe some correlation on the effect of mutation (i.e., DNA conformational change due to mutation). Comparison of Fig. 9 (model m1) and Fig. 8 (model m0) reveals that there is no big difference between these two models. The distance distribution behavior is similar for most of the nucleotides, although there is seen a little fluctuation in T5, G19, etc. The largest structure changes (i.e., the highest degree of the distance distribution values) could be seen comparing the models m0

Model m3: T4G and A17C mutations

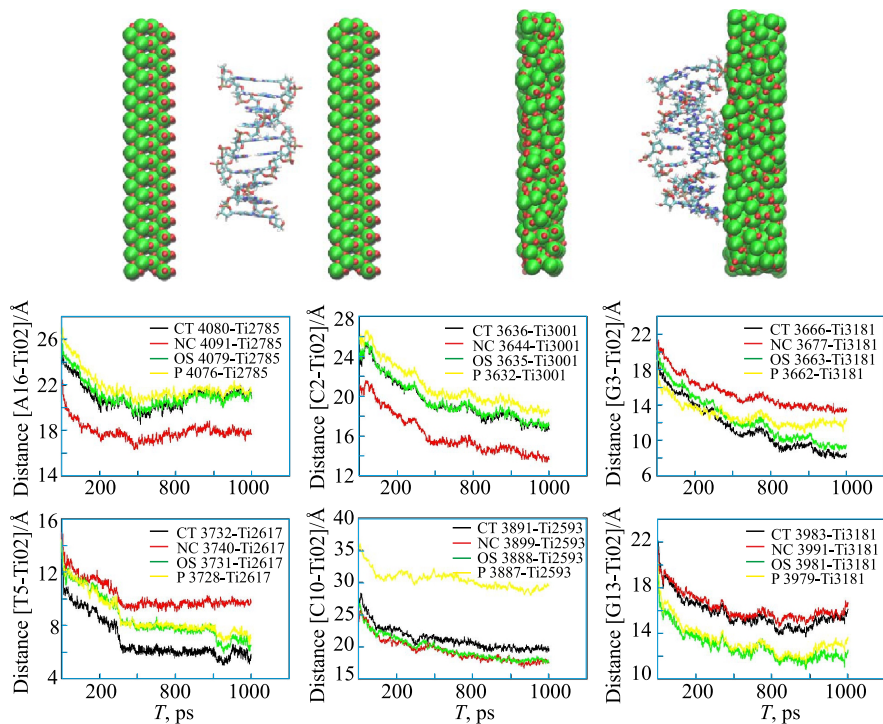


Fig. 11. The initial and final DNA configurations for model m3 (T4G and A17C mutations) as well as for the RMSD graphs are shown

and m2. From Fig. 10 (model m2) and Fig. 8 (model m0), the difference in the values of DNA–surface distances may reach 15 or 16 Å. Additionally, the m2 closest atom to TiO<sub>2</sub> surface is oxygen instead of nitrogen as for m0. Moreover, the distance distributions have a relatively wide profile if to make comparison between similar nucleotides. Thus, for the model m2, one observes a relatively high structure deformation degree which is likely due to more intense DNA interaction with TiO<sub>2</sub> surface. From Figs. 8 (model m0) and 11 (model m3), we predict some similarities between m2 and m3 conformations in accordance to the mutation type in both. Estimating the DNA–TiO<sub>2</sub> surface interaction, based on the distance graphs (Figs. 8–11), one can now summarize which structure has the highest tendency to interact with TiO<sub>2</sub>.

From the net change in distances between the DNA and TiO<sub>2</sub> atoms, we calculated  $\Delta D$ , the difference between the upper and lower values of the close contact distances in four DNA structures. The values of  $\Delta D$  are summarized

**Table 3. The DNA–TiO<sub>2</sub> distance distributions averaged between the four DNA models as presented in Fig.5 and Table 2**

| Nucleotide/structure | Model m0 | Model m1 | Model m2 | Model m3 |
|----------------------|----------|----------|----------|----------|
| A6                   | 8.00     | 11.0     | —        | 8.00     |
| A7                   | —        | —        | 12.0     | 4.00     |
| A16                  | 14.0     | 11.0     | 12.5     | 19.0     |
| A17                  | 14.0     | 14.0     | 12.5     | —        |
| C2                   | 11.0     | 13.0     | 11.0     | 12.0     |
| C10                  | 10.0     | 11.0     | 14.0     | 17.0     |
| C18                  | 10.5     | 12.0     | 14.5     | 9.00     |
| G3                   | 10.0     | 10.0     | 8.00     | 12.5     |
| G13                  | 11.5     | 8.00     | 8.00     | 10.0     |
| G19                  | 9.00     | 11.5     | 9.50     | 8.50     |
| T4                   | 13.0     | 8.00     | 13.0     | —        |
| T5                   | 19.5     | 5.00     | 19.5     | 9.50     |
| T14                  | 11.0     | 11.0     | 11.0     | 10.0     |
| T15                  | —        | —        | —        | 13.0     |
| Average value        | 11.0     | 10.5     | 12.1     | 11.0     |

in Table 2 for all DNA models. The structure that possesses the highest value of  $\Delta D$  has to be the most flexible one — the most deformable structure due to the interaction with the surface. From Table 2, the DNA structure in the mutation model m2 has the highest value of  $\Delta D$  implying that DNA molecule in model m2 has probably more strongly interacts with TiO<sub>2</sub> surface than in the other one.

## CONCLUSION

In the present paper, long-nanosecond MD simulations were performed for four DNA small chains (models m0–m3) to elucidate the effect of induced mutations on the DNA–water–NPs and DNA–water–TiO<sub>2</sub> surface interactions. First, for the DNA–metallic NP interaction, we have observed and energetically estimated the NP preferable binding site to DNA structure located on its minor and major grooves. Until NP binds to DNA, the DNA conformation behaves stable and it does not change visibly in comparison with the DNA starting one. From the stage of the DNA–NP bond formation, the DNA structure undergoes a substantial deformation. The shape of the DNA molecule would continuously change in correlation with the NP capture and formation of a close contact.

Next we extended the DNA–NPs interaction mechanism to the DNA–TiO<sub>2</sub> surfaces one. We have generated four DNA structures interacting in water solvent with NP. The changes in the DNA–surface distance distributions were estimated as an indicator for the degree of DNA conformation behavior during the ap-

proaching TiO<sub>2</sub> surface. The major observations include the following: a) The closest atoms to TiO<sub>2</sub> are nitrogen and oxygen as predicted due to formation of coordination bonds with Ti ion; b) The DNA structure to be distinguished by its essential conformation changes compared with the native one has to be model m2; the others follow this order m2 > m3 > m1; c) As predicted G1 → C1 mutation does not visibly affect the DNA–surface distance distributions; d) All this mutation nearly does not affect the closest atom or, in some cases, nitrogen and oxygen atoms alternate with each other; e) For m2 model, the largest increase in the DNA–surface distance profiles was observed in T5 site; the difference between the contact distances compared to that of m0 one could reach 15 or 16 Å.

In summary, the DNA conformation has to change essentially as the nanoparticle has been captured by a DNA specific site. As the DNA–nanoparticle(s) cluster together with the nanoparticle(s) may pull the strands of DNA apart. The specific DNA sites that we mutated belong to a binding site that can efficiently capture the metallic nanoparticle(s). The DNA–TiO<sub>2</sub> interaction are likely subjected to a similar mechanism as for the DNA–nanoparticle(s) ones. So far, the DNA conformational changes under TiO<sub>2</sub> interactions possess a different nature with regard to four DNA structures.

**Acknowledgements.** This work has been performed in the framework of joint collaborative agreement: Arab Republic of Egypt (ARE)–Joint Institute for Nuclear Research (JINR) (project #302). This work is a part of collaboration between JINR (Russia), RIKEN (Japan), and Keio University (Japan). The work has been performed within a research collaboration between JINR (Russia) and Keio University (Japan) and was supported by the JSPS (Japan Society for the Promotion of Science)–RFBR (Russian Foundation for Basic Research) (grant No.13-04-92100). The work has been supported in part by the Grant in Aid for the Global Center of Excellence Program to the Center for Education and Research of Symbiotic, Safe and Secure System Design from Japan’s Ministry of Education, Culture, Sport, and Technology.

The MD simulations have been performed using computer software, hardware facilities, and cluster machines at the CICC (JINR), RICC (RIKEN), and the Yasuoka Laboratory of Keio University (Japan). The authors would like to specially thank Sergei Negovellov (JINR) for technical assistance and helpful comments.

## REFERENCES

1. *Vinall R. L. et al.* The R273H p53 Mutation Can Facilitate the Androgen-Independent Growth of LNCaP by a Mechanism that Involves H2 Relaxin and Its Cognate Receptor LGR7 // *Oncogene*. 2006. V. 25. P. 2082–2093.
2. *Molecular Dynamics of Nanobiostuctures / Ed. Kholmurodov Kh.* Nova Science Publishers Ltd., 2011. ISBN: 978-1-61324-320-6. 230 p.

3. *Kholmurodov Kh.T., Fel'dman T.B., Ostrovskii M.A.* Molecular Dynamics of Rhodopsin and Free Opsin: Computer Simulation // *Neuroscience and Behavioral Physiology*. 2007. V. 37(2). P. 161–174.
4. *Pearlman D.A. et al.* AMBER, a Computer Program for Applying Molecular Mechanics, Normal Mode Analysis, Molecular Dynamics and Free Energy Calculations to Elucidate the Structures and Energies of Molecules // *Comp. Phys. Commun.* 1995. V. 91. P. 1–41.
5. *Case D. C. et al.* // AMBER, 2010.
6. *Cornell W.D. et al.* A Second Generation Fortran Field for the Simulation of Proteins and Nucleic Acids // *J. Am. Chem. Soc.* 1995. V. 117. P. 5179–5197.
7. *Humphrey W., Dalke A., Schulten K.* VMD — Visual Molecular Dynamics // *J. Mol. Graphics*. 1996. V. 14. P. 33–38.
8. *Kholmurodov K. et al.* A Smooth-Particle Mesh Ewald Method for DL-POLY Molecular Dynamics Simulation Package on the Fujitsu VPP700 // *J. Comp. Chem.* 2000. V. 21. P. 1187, 3.
9. *Kholmurodov Kh.T., Dushanov E.B., Yasuoka K.* MD Simulations of the P53 Oncoprotein Structure: The Effect of the Arg273His Mutation on the DNA Binding Domain // *Advances in Bioscience and Biotechnology*. V. 2, No. 5. ISSN Print: 2156-8456 ISSN Online: 2156-8502 (2011).
10. *Selwyne R. A., Kholmurodov Kh. T., Koltovaya N. A.* Homology Modelling and Molecular Dynamics of Cyclin-Dependent Protein Kinases // *IT for Real World Problems (Universities Press Series in Systems, Models, Informatics and Control) / Ed. Sree Hari Rao. Universities Press (India) Private Ltd., 2011. P. 1–72.*
11. *Kholmurodov Kh.T. et al.* MD Simulations on the Structure of Oncoproteins P53: Wild-Type and Radioresistant Mutant Systems // *Molecular Dynamics of Nanobiostructures*. N. Y.: Nova Science Publishers, 2011. ISBN: 978-1-61324-320-6.
12. *Narumi T. et al.* Molecular Dynamics Machine: Special-Purpose Computer for Molecular Dynamics Simulations // *Molecular Simulation*. 1999. V. 21. P. 401–408;  
*Narumi T. et al.* // MDM Version of AMBER, 2000;  
*Narumi T. et al.* 46 TFLOPS Special-Purpose Computer for Molecular Dynamics Simulations: (WINE-2) // *Proc. of the 5th Intern. Conf. on Signal Processing*. Beijing, 2000. P. 575–582;  
*Susukita R. et al.* Hardware Accelerator for Molecular Dynamics: MDGRAPE-2 // *Comp. Phys. Commun.* 2003. V. 155. P. 115–131.
13. *Taiji M. et al.* Protein Explorer: A Petaflops Special-Purpose Computer System for Molecular Dynamics Simulations // *Proc. of SC2003, Phoenix, AZ 2003*;  
*Narumi T. et al.* A High-Speed Special-Purpose Computer for Molecular Dynamics Simulations: MDGRAPE-3 // *Proc. of NIC Workshop 2006. Comp. Biophys. to Syst. Biology. NIC Series*. 2006. V. 34. P. 29–35;  
*Narumi T. et al.* A 185 TFLOPS Simulation of Amyloid-Forming Peptides from Yeast Prion Sup35 with the Special-Purpose Computer System MDGRAPE-3 // *Proc. of SC2006, Tampa, FL, 2006.*
14. *Diebold U.* The Surface Science of Titanium Dioxide // *Surf. Sci. Rep.* 2003. V. 48. P. 53–229.

15. Monti S., Carravetta V., Zhang W., Yang J. Effects due to Interadsorbate Interactions on the Dipeptide/TiO<sub>2</sub> Surface Binding Mechanism Investigated by Molecular Dynamics Simulations // *J. Phys. Chem. C*. 2007. V. 111. P. 7765–7771.
16. SantaLucia J. (Jr.). A Unified View of Polymer, Dumbbell, and Oligonucleotide DNA Nearest-Neighbor Thermodynamics // *Biochemistry*. 1998. V. 95. P. 1460–1465.
17. Tulpan D., Andronesu M., Leger S. Free Energy Estimation of Short DNA Duplex Hybridizations // *BMC Bioinformatics*. 2010. V. 11. P. 105.
18. SantaLucia J. (Jr.), Hicks D. The Thermodynamics of DNA Structural Motifs // *Ann. Rev. Biophys. Biomol. Struct.* 2004. P. 415–440.
19. Breslauert K.J. et al. Predicting DNA Duplex Stability from the Base Sequence // *Biochemistry*. 1986. V. 83. P. 3746–3750.
20. Freyre-Fonseca V. et al. Titanium Dioxide Nanoparticles Impair Lung Mitochondrial Function // *Toxicology Letters*. 2011. V. 202. P. 111–119.
21. Trouiller B. et al. Titanium Dioxide Nanoparticles Induce DNA Damage and Genetic Instability in vivo in Mice // *Cancer Res*. 2009. V. 69(22).
22. Saquib Q. et al. Titanium Dioxide Nanoparticles Induced Cytotoxicity, Oxidative Stress and DNA Damage in Human Amnion Epithelial (WISH) Cells // *Toxicology in vitro*. 2012. V. 26. P. 351–361.
23. Trouiller B. et al. Titanium Dioxide Nanoparticles Induce DNA Damage and Genetic Instability in vivo in Mice // *Cancer Res*. 2009. V. 69. P. 8784–8789.
24. Dunford R. et al. Chemical Oxidation and DNA Damage Catalyzed by Inorganic Sunscreen Ingredients // *FEBS Letters*. 1997. V. 418. P. 87–90.
25. Roy S., Sen S. Exploring the Potential of Complex Formation between a Mutant DNA and the Wild-Type Protein Counterpart: A MM and MD Simulation Approach // *J. Mol. Graphics and Modelling*. 2006. V. 25. P. 158–168.
26. Todorov I. T. et al. DL-POLY\_3: New Dimensions in Molecular Dynamics Simulations via Massive Parallelism // *J. Mater. Chem*. 2006. V. 16(20). P. 1911–1918.
27. Jorgensen W.L., Chandrasekhar J., Madura J.D. Comparison of Simple Potential Functions for Simulating Liquid Water // *J. Chem. Phys.* 1983. V. 79. P. 926–935.
28. Brooks B.R. et al. CHARMM: The Biomolecular Simulation Program // *J. Comp. Chem*. 2009. V. 30(10). P. 1545–1614.
29. Ryckaert J.P., Ciccotti G., Berendsen H.J.C. Numerical Integration of the Cartesian Equations of Proteins and Nucleic Acids // *J. Comp. Phys.* 1997. V. 23. P. 327–341.
30. Kavathekar R.S. et al. Molecular Dynamics Study of Water in Contact with the TiO<sub>2</sub> Rutile-110, 100, 101, 001 and Anatase-101, 001 Surface // *Mol. Phys.* 2011. V. 109(13). P. 1649–1656.
31. Guillot B., Sator N. A Computer Simulation Study of Natural Silicate Melts. Part I: Low Pressure Properties // *Geochimica et Cosmochimica Acta*. 2007. V. 71(5). P. 1249–1265.
32. Matsui M., Akaogi M. Molecular Dynamics Simulation of the Structural and Physical Properties of the Four Polymorphs of TiO<sub>2</sub> // *Mol. Simulation*. 1991. V. 6(4-6). P. 239–244.
33. WWW-MINCRYST. Crystallographic and Crystallochemical Database for Minerals and Their Structural Analogues. <http://database.iem.ac.ru/mincryst/>

Received on February 25, 2013.

Корректор *Т. Е. Попеко*

Подписано в печать 30.04.2013.

Формат 60 × 90/16. Бумага офсетная. Печать офсетная.

Усл. печ. л. 1,43. Уч.-изд. л. 1,93. Тираж 205 экз. Заказ № 57985.

Издательский отдел Объединенного института ядерных исследований  
141980, г. Дубна, Московская обл., ул. Жолио-Кюри, 6.

E-mail: [publish@jinr.ru](mailto:publish@jinr.ru)

[www.jinr.ru/publish/](http://www.jinr.ru/publish/)